High-Efficiency Omnidirectional Broadband Light-Management Coating Using the Hierarchical Ordered-disorder Nanostructures with Ultra Mechanochemical Resistance

*Shengjie Zhai, Yihong Zhao, and Hui Zhao**

Department of Mechanical Engineering, University of Nevada Las Vegas, Las Vegas, Nevada 89154-4027, USA

Corresponding Author

**Email: hui.zhao@unlv.edu*

ABSTRACT

High-efficient light-management nanostructures are critical to various optical applications. However, in practical implementation, these structures have been limited by the needs to resist mechanical abrasion, erosion, chemical exposure, ultraviolet radiation, and performance deterioration by dust accumulation. To address these critical technological gaps, we herein report a conceptually different approach, employing a hierarchical nanostructure embedded with multilayer LightScribe-etched graphene (LSEG), capable of omnidirectional broadband light management with both high optical transparency (>90%) and high haze (~89%), ideal for photovoltaics, which simultaneously demonstrates extraordinary robustness to various environmental challenges ranging from mechanical abrasion, UV exposure, corrosions, outdoor exposures, to resistance to dust accumulation. The reported nanostructures can be readily

combined to any optoelectrical devices' surface and the practical tests on coated amorphous silicon (a-Si) solar cells show that it outperforms the state-of-art commercial coating by maintaining both 10% efficiency improvement along with the prevention of dust accumulation in contrast to 56.2% efficiency degradation with the commercial coating after the one-month outdoor test.

KEYWORDS: multifunctionality, ordered-disorder nanostructures, omnidirectional light management, durability, LightScribe-etched graphene

1. Introduction

Broadband light-management nanostructures have been developed and investigated as a versatile component by both academic research and industrial development for broad technological applications ranging from thin-film photovoltaics, photoelectric sensors, photoelectrochemical cells, and solar-to-thermal technologies.[1–5] Most of these light-management nanostructures are made from polymer due to low cost, excellent mechanical flexibility, and simple scale-up production.[6] However, the lack of robustness and poor dust tolerance under various environmental challenges impose the critical challenges for the practical implementation, in particular, for flexible or portable photovoltaic systems where the conventional protection glass or other package layers are not desirable, because many of the characteristics, giving rise to the extraordinary light-management properties, also simultaneously cause the durability issue. For example, the dedicate nanostructures that lead to light trapping can be easily damaged by mechanical abrasion, conditions commonly encountered in outdoor with dust intrusion.[7] Once damaged, the light trapping effect deteriorates. Excellent chemical resistance is also important in terms of acid rain and other harsh environments. In addition, the polymer can degrade when exposed to prolonged ultraviolet. The durability clearly cannot be trade-offs in even a substantial efficiency enhancement

promised by nanostructures. Finally, just as importantly, the capability of preventing dust accumulation that can obscure light management and significantly decrease efficiency is another critical issue for practical applications. Therefore, despite enormous progress, durable light-management nanostructures have remained elusive.

Learning from Nature

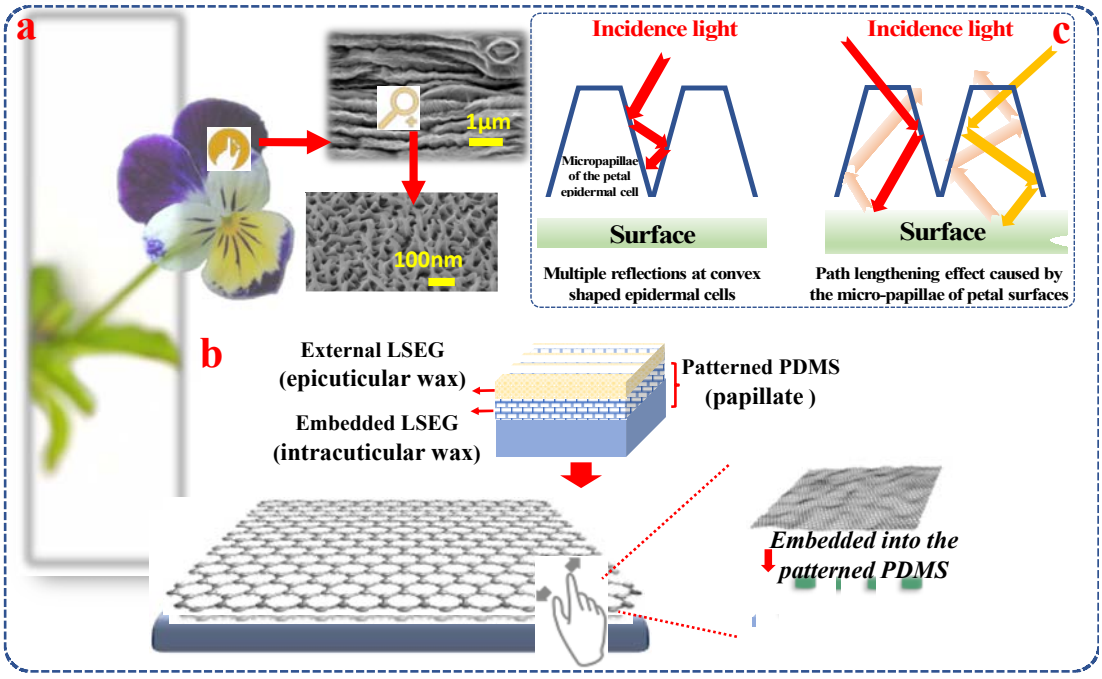

Figure 1. (a) The image of the Viola tricolor petal at the different scales; **(b)** The schematic view of the hierarchical structure of our Viola tricolor inspired design; **(c)** The light-trapping mechanisms possessed by the Viola Tricolor.

To tackle this critical technological gap, we resort to nature where a billion years of evolution provides us ideas. To maximize the attractiveness for pollinators, petals adapted to trap more lights in both visible and the UV spectral range. The more light strikes on a pigment, the more intense the color signal will be.[8,9] In particular, Viola tricolor petals, which live in the harsh environments including uncultivated areas in gardens, barren ground, waste areas with sparse vegetation in

partial shade, exhibit both exceptional durable light trapping effects and the prevention of dust accumulation under harsh environments (**Figure 1**).[10]

The exceptional light-trapping capability of Viola tricolor petal can be attributed to two main mechanisms related to its evolved hierarchical structure (ordered-disorder),[11–13] which includes papillate epidermal cells (ordered structure), cuticular folding, and the outer layer of wax pruinosity (**Figure 1b**). Due to the irregular arranged transparent stacked wax pruinosity featuring with random height (disordered structure), the undesired Fresnel reflection can be effectively suppressed over a broad range of wavelengths, and the petal exhibits the omnidirectional light trapping property by velvet-like sculptures (**Figure 1c**).[13,14] Moreover, the light can be effectively diffusely scattered inside the petal epidermal cells, increasing the path of transmitted light. In this way, ambient light can be more efficiently collected omnidirectionally by Viola tricolor petal in a shady environment. Recently by coating the structures directly replicated from the Viola flowers on crystalline silicon solar cells, a 6% percent improvement in power conversion efficiency was observed due to the broadband enhancement from the optical properties of the Viola texture with a hierarchical structure.[15]

Even more interestingly, Viola tricolor does not exhibit the typical petal effect (water droplets do not roll off when tilted).[16,17] Instead, it possesses water-repellency capability like the lotus leaves, which is attributed to the epidermal cells with the fine cuticular folding (surface roughness) and the hydrophobic wax layer (hydrophobic surface chemistry). The surface roughness and the hydrophobic layer are the two essential factors responsible for water repellency that can effectively prevent dust accumulation.[18] The durability of Viola tricolor surviving in harsh environments is due to the continuous dense wax-flake layer excreted by epidermal cells which effectively reduces the damage and protects the surface from harsh environmental stresses such as solar irradiation,

mechanical abrasion, and corrosion.[19] Furthermore, the intracuticular wax layer that is stably embedded with cutin into the cuticle[20–22] provides additional durability against the damages of friction and over-irradiation exposure.[22]

In summary, the integration of papillae and cuticular folding with the embedded continuous dense wax-flake layer (ordered disorder) in Viola tricolor petal is identified for the exceptional omnidirectional broadband light management and the prevention of dust accumulation with robust durability and longevity.

Rational for multilayer graphene

Learning from Viola tricolor petals, we, herein, report a method to fuse the multilayer graphene (disordered) with papillae-like nanostructures (ordered) to achieve the aforementioned exceptional properties of Viola tricolor petal for durable light-management (**Figure 1b**). We chose the multilayer graphene based on the following criteria: (1) graphene, itself has the excellent chemical resistance (acid/base/salt), impermeability to gases, superb mechanical strength, thermal stability, and high specific surface areas;[23–26] (2) the multilayer graphene can be self-assembled into folding structures that can mimic the cuticular foldings; (3) the multilayer graphene itself is dense and continuous and can be embedded into the underneath structures, similar to the wax-flake layer as shown in **Figure 2a** and **Figure 2b** via our fabrication process. Even more interestingly, recent studies discovered that thin conductive carbon materials could induce hot electron effects that may increase the scattering much stronger than traditional Rayleigh scattering and lower the absorption.[27,28] In addition, the rough and porous multilayer surface can also effectively decrease the reflection.[29] In other words, the multilayer graphene can go beyond their natural counterpart, Viola tricolor petals, by taking advantage of the exceptional properties such as the hot electron effects in graphene, to further improve the efficiency.

2. Results and Discussions

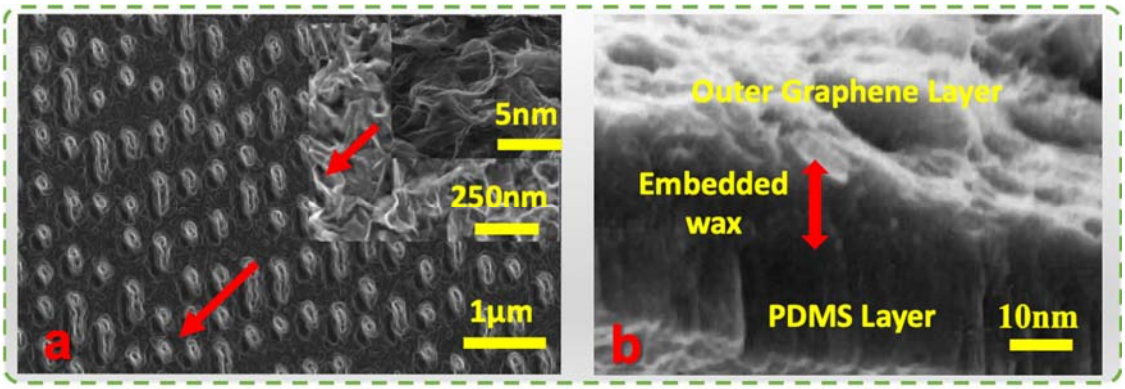

Figure 2 (a) The SEM images of the bioinspired LSEG-enabled ordered-disorder nanostructure; **(b)** The SEM image of the embedded intracuticular wax-liked graphene layer.

Figure 3 describes the schematics of the fabrication process. Detailed procedures can be found in the experimental section. Here, we briefly highlight the key steps. First, a thin layer of poly(dimethylsiloxane) (PDMS), which includes the designed ordered papillate-like structures, is made by the soft lithography.[30] Next, a graphene oxide layer is dispersed onto the PDMS layer by spin-coating, which is attached to a LightScribe optical disc. By burning process under laser irradiation, the well-formed graphene oxide layer is successfully reduced to LightScribe-etched graphene (LSEG) layer.[31] Finally, calcination at 400°C can remove surface contamination and improve the transparency (**Figure S1**).[32]

To examine if oxygen is effectively removed in LSEG, **Figure 4** shows the EDS spectra, WDS spectra and Raman spectra of the graphene layer before and after the laser scribing. All three measurements suggest that the graphene oxide has been successfully reduced to graphene. For example, in Raman spectra, both the increase of the intensity ratio of D/G and the blue shift of the D band peak are due to the successful reduction of graphene oxide.[33–36]

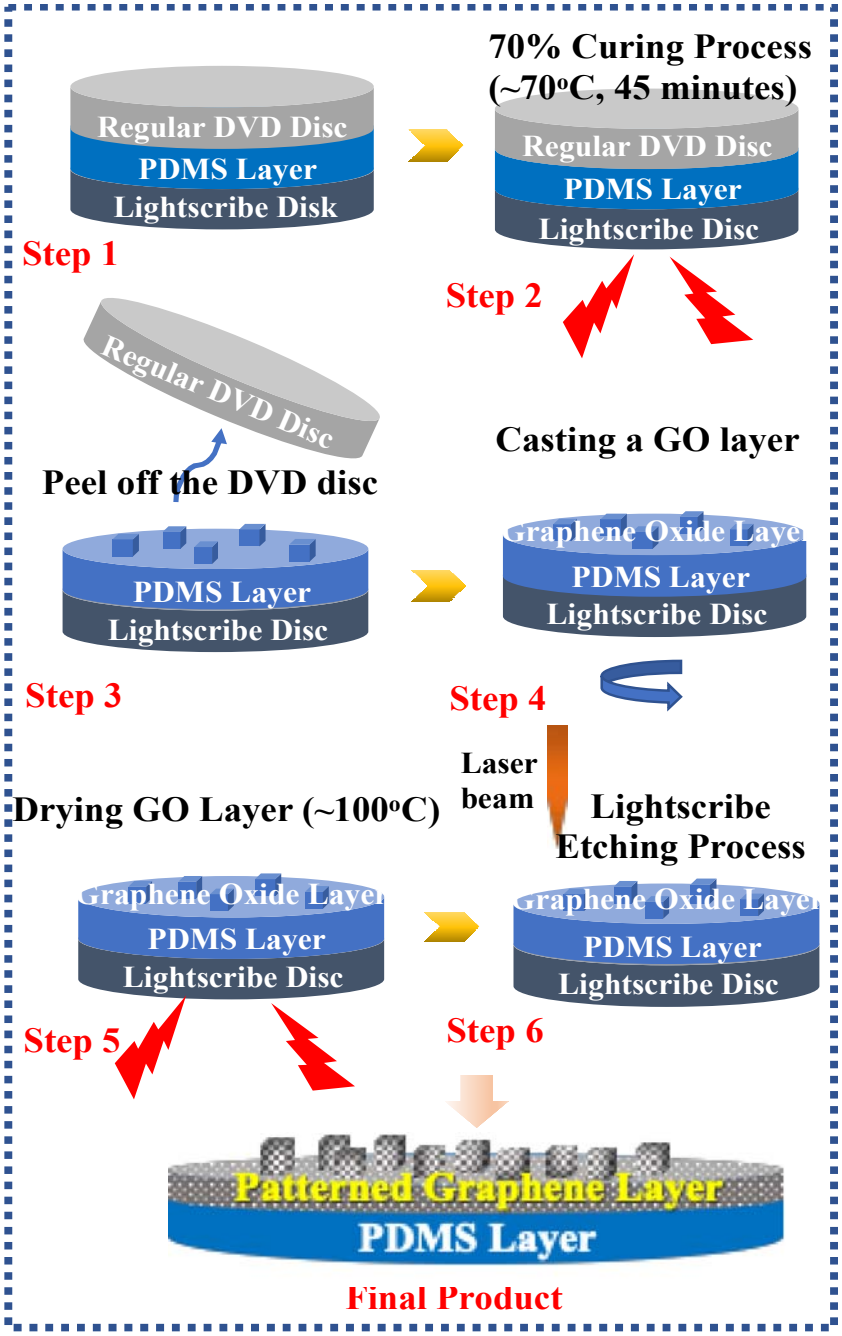

Figure 3. The schematics of the LightScribe etching process.

Our method is an all-solid-state one that prevents the restacking of graphene sheets caused by strong van der Waals interaction forces. This restacking commonly happens during traditional wet-chemical graphene reduction methods. In contrast, the LightScribe etching induces the

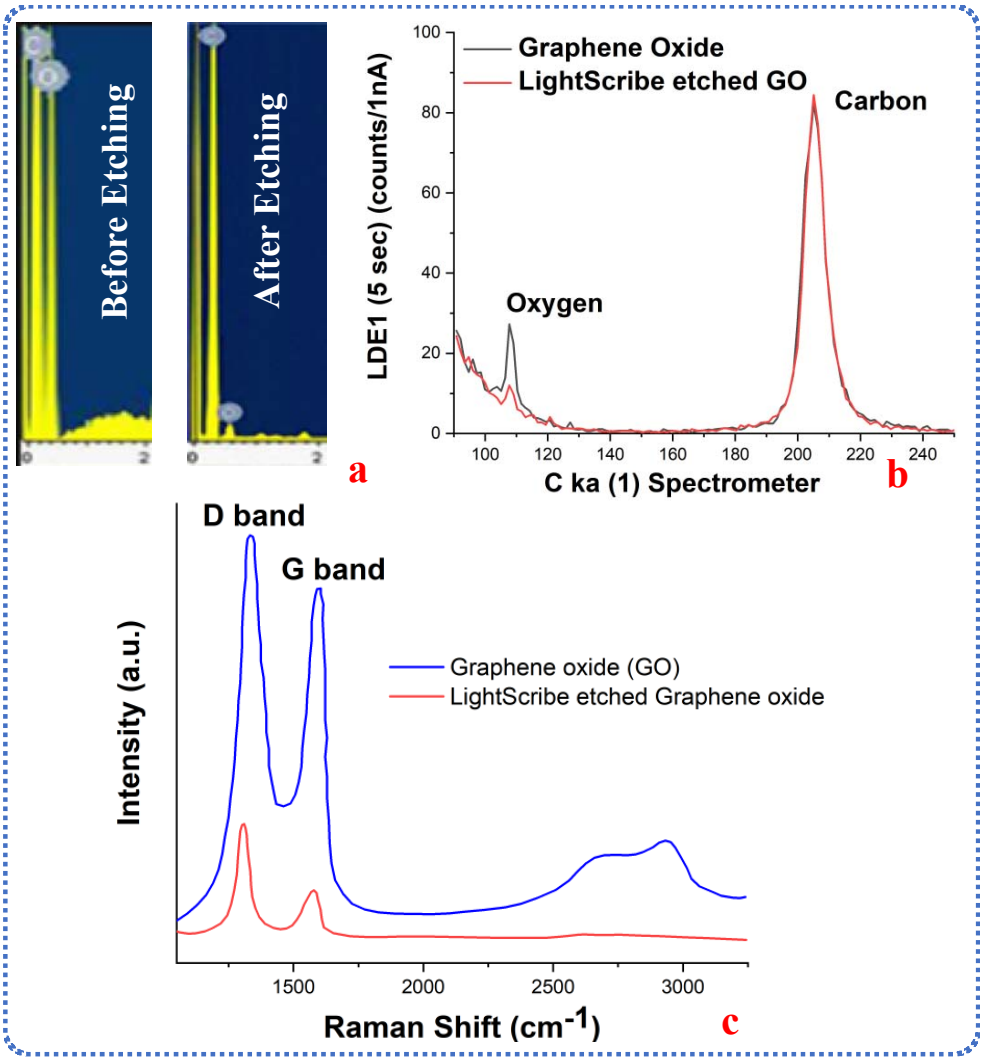

Figure 4 (a) The EDS spectra; (**b**) the wavelength-dispersive X-Ray spectra (WDS); and (**c**) the Raman Spectra of the graphene layer before and after the LightScribe etching.

simultaneous reduction and exfoliation of graphene oxide sheets and creates more open pores. Those open pores can trap air, increase roughness, and promote water repellency. Also, the multilayer LSEG traps additional air among the graphene layers.[37] These additional air films among the various types of graphene layers can resist water intrusion to further improve the durability (**Figure 5a**).

We must emphasize that our presented bioinspired strategy is conceptually different from other

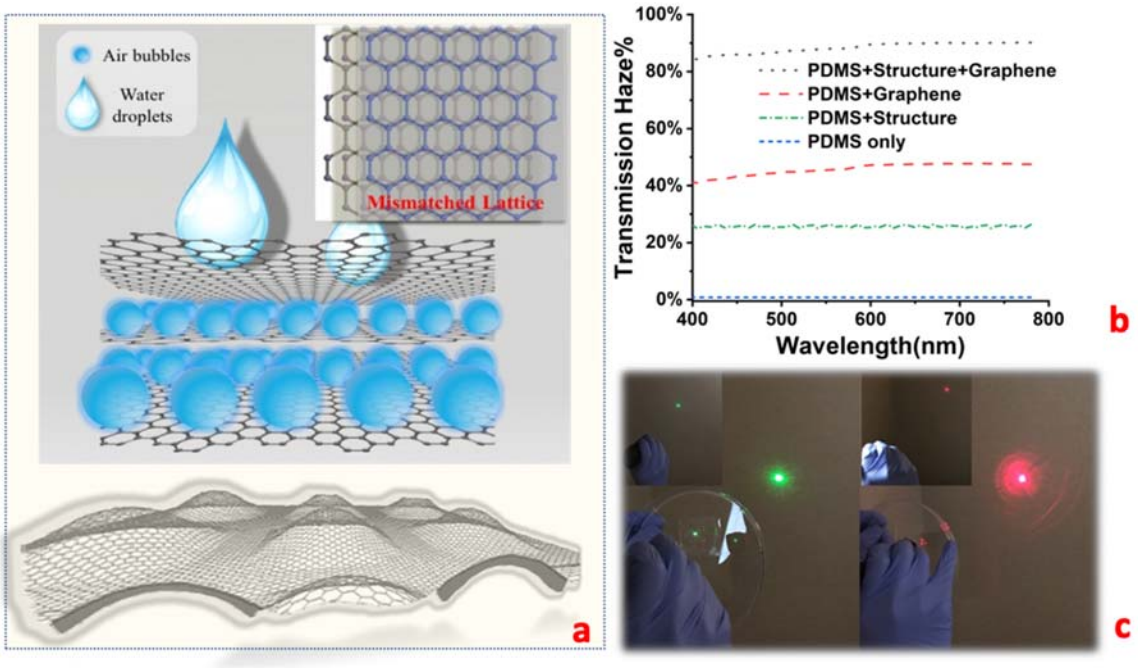

Figure 5 (a) The schematics of trapped air bubbles between mismatched lattice graphene layers to prevent water intrusion; **(b)** The transmittance haze as a function of the wavelength for various surfaces; **(c)** The light scattering effects with a 532nm (left side), and a 671nm (right side) laser sources;

synthetic bioinspired methods which mainly focus on the structural aspect that does not truly capture the main features of natural petals. In contrast, by implanting a thin layer of LSEG into the underneath PDMS papillated structures before completely cured under the high-vacuum environment (~10^{-7} Pa), the graphene layer is embedded into the PDMS and result in an "intracuticular" graphene layer to make the LSEG layer similar to the natural wax layer (**Figure 2b**). Because the LSEG layers only have a thickness of tens nm, the original structure on the PDMS, which has a hundreds-nm size (subwavelength), can be maintained (**Figure 2a**).

Optical properties

As discussed before, for Viola tricolor petals, the incident light scatters as it propagates through, leading to excellent light trapping effects. It is, therefore, worthwhile to investigate whether the fabricated multilayer LSEG with a refractive index of 2.3[38] can effectively scatter the light and increase the diffuse paths. To quantify the light scattering, the optical haze measurements were carried out by the Jasco V670 with the integrated sphere.[39] The transparent haze describes the amount of light scattering when light passes. It is defined as the percentage of transmitted light by forwarding scattering. **Figure 5b** plots the transmittance haze as a function of the wavelength. A transmission haze close to 89% is demonstrated over a broad range of wavelength. High transmission haze can effectively increase light scattering, improve the light absorption and solar cell efficiency. For comparison, in **Figure 5b**, we also measured the transmission haze over a flat PDMS layer coated with LSEG, which is around 47%, and the transmission haze over a structured PDMS layer without LSEG, around 24%. Evidently, the high transmission haze is due to the unique integration of the ordered and disordered nanostructures.

The light scattering effect can also be visualized by lasers with a wavelength of 671 nm and 532 nm with a beam diameter of 0.3 cm that pass through the designed ordered-disorder nanostructure and form a larger illuminated circular area with a diameter of 8 cm on the target surface which is 50 cm away (**Figure 5c**). The same experiments were also applied to a flat PDMS and a structured PDMS without the LSEG. The illuminated areas did not change that much, shown in Supporting Information **Figure S2**. The increased scattering can be attributed to the mismatched lattice multilayer graphene, which can effectively scatter and trap the light,[40] and airs trapped inside LSEG, which act like adaptive focus lenses to collimate the incident light.[41]

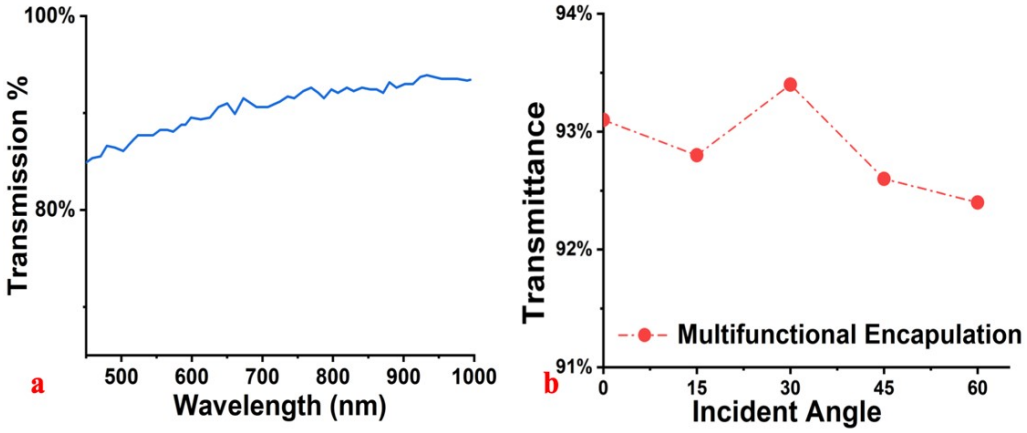

Figure 6 The transmittance of the LSEG-enabled order-disorder nanostructure as a function of wavelength (**a**) and under a wide range of the incident light angle (**b**).

Finally, **Figure 6** shows the transmittance as a function of wavelength and the total transmittance as a function of incident angle. Evidently, the LESG-enabled nanostructure also maintains the high transmission (>90%) over a broad range of angle, suggesting the omnidirectionality. In other words, our LSEG-enabled structured layer achieves both high transmittance and high transmission haze simultaneously, crucial to photovoltaic applications.[39]

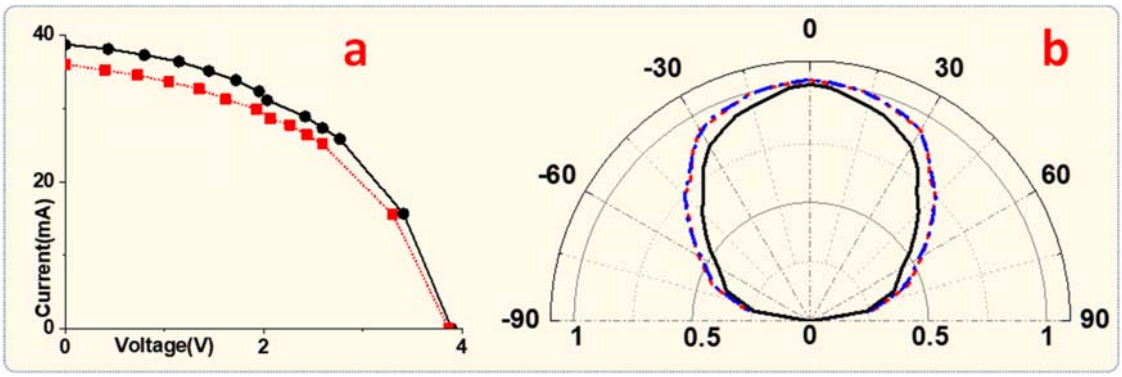

Figure 7 (a) The I-V curves of a thin-film solar cell with (the solid line with black circles) and without (the dashed line with red squares) the designed coating with 10% improvement; **(b)** The angular dependence of a normalized photocurrent with (dashed and dot-dashed lines) and without (solid line) the designed coating, showing omnidirectional optical properties. The blue dashed line and the red dot-dashed line represent two different horizontal positions of the solar cell, with 90° of separation.

Now as an example to demonstrate its light-management capability, we attach the LSEG-enabled ordered-disorder nanostructure with a thin-film amorphous silicon solar cell module manufactured by PowerFilm Inc (**Figure S3**). We recorded the I-V curves of the solar cell as well as for the same cell with the LSEG-enabled nanostructure and computed the efficiency under a solar simulator with 1 Sun AM 1.5-G illumination. **Figure 7a** shows that the nanostructure can enhance efficiency by 10% due to the increase in the short-circuit current by reducing the reflection (see **Figure S4**) and capturing diffuse illumination. The photocurrents were recorded under illumination from various incident angles by rotating the device gradually. **Figure 7b** shows the measured angular dependence of short-circuit photocurrent. Here, the incident angle is defined as the one between the incident light and the normal direction of the device. For illustration purposes, the short-circuit current was normalized with the value from the solar cell without the nanostructure under zero-incident-angle illumination. **Figure 7b** indicates that a larger photocurrent improvement of over 10% was observed in a wide incident-angle range of 0^{o}-80^{o}, suggesting an omnidirectional distribution of redirected incident lights. The blue dashed line and the red dot-dashed line represent two different horizontal positions of the solar cell, with 90^{o} of separation. The collapse of the two lines suggests that our nanostructured coating was uniformly distributed with little defect.

Water repellency

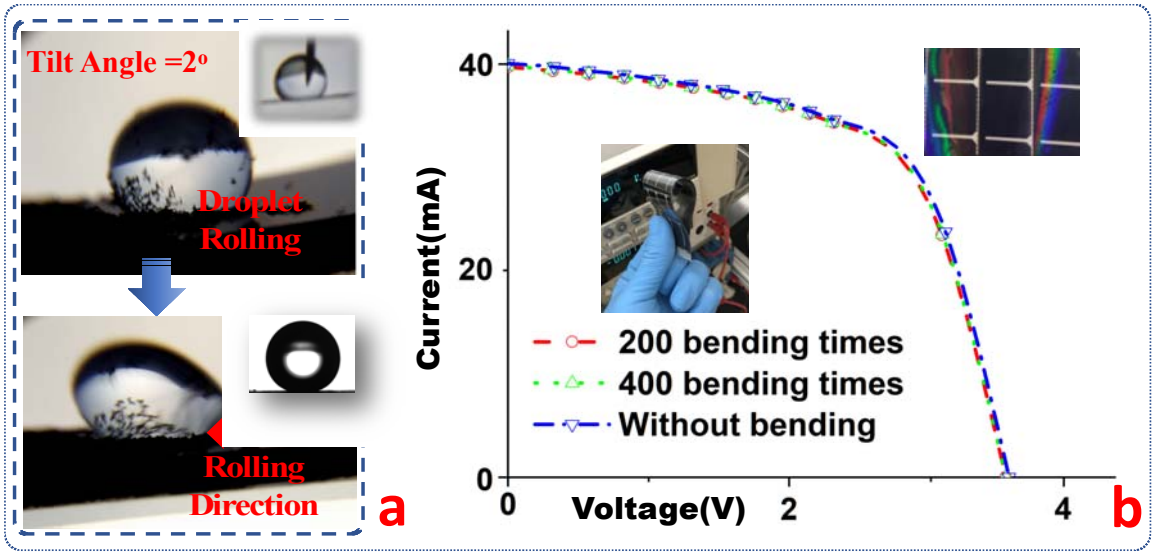

Figure 8 (a) The water droplet wipes the dirt away from the surface with a titled angle of 2°. The insert shows that the droplet has a contact angle of 158°; **(b)** The I-V curves before and after 200 and 400 bending times. The insert shows the photograph of the bended solar cell coated with the LSEG-enabled ordered-disorder nanostructure.

It is recognized that dust accumulation not only significantly affects the optoelectronic systems' efficiency but also can permanently damage their surface.[42] Therefore, a water-repellency surface becomes a key towards durable optoelectronic systems. Here we deposit a 5 µL droplet over the LESG-enabled surface and demonstrate that similar to Viola tricolor petals, our LSEG-enabled nanostructured surface exhibits the lotus effect with a contact angle of 158° degree and roll-off angle about 2° degrees as shown in **Figure 8a** and **Figure S5**. In addition, to demonstrate self-cleaning, **Figure 8a** also shows that the water droplet effectively picked up the dirt due to the stronger adhesion force between the dirt and the water in comparison with the one between the dirt and the synthesized surface and carried them away (detailed shown in **Figure S6**).

Moreover, considering the flexibility is a crucial feature of the soft optoelectronic devices, it is worthwhile to examine whether the LSEG-enabled ordered-disorder nanostructure changes the

bendability and influences efficiency. **Figure 8b** shows the photograph of the flexibility of our LSEG-enabled coating. Evidentially, our LSEG coating does not modify the bendability after hundreds of bending tests. We recorded the I-V curves after bending by the mechanical force. The effect of the bending cycles on the photovoltaic performance is presented in **Figure 8b**. The results show that the short circuit current and open circuit voltage almost remain the same during the bending tests. We also measured the contact angles after bending, showing that the contact angle stays almost the same (shown in **Figure S7**).

Various durability tests

Finally, we carried out a series of well-designed durability tests to systematically characterize the robustness. The durability tests here can be categorized into: (1) resistance to the dynamic impact; (2) resistance to UV; (3) resistance to corrosion; (4) resistance to harsh outdoor natural desert conditions. In the following, we described them, one by one.

Solid particle test: An essential category of durability test is under the dynamic impact of the solid phase. The test was designed for testing the feasibility of the LSEG-enabled ordered-disorder nanostructure in outdoor applications where they have to face harsh weather conditions and contamination or degradation by dynamic collision with dust particles. Two types of sand grains

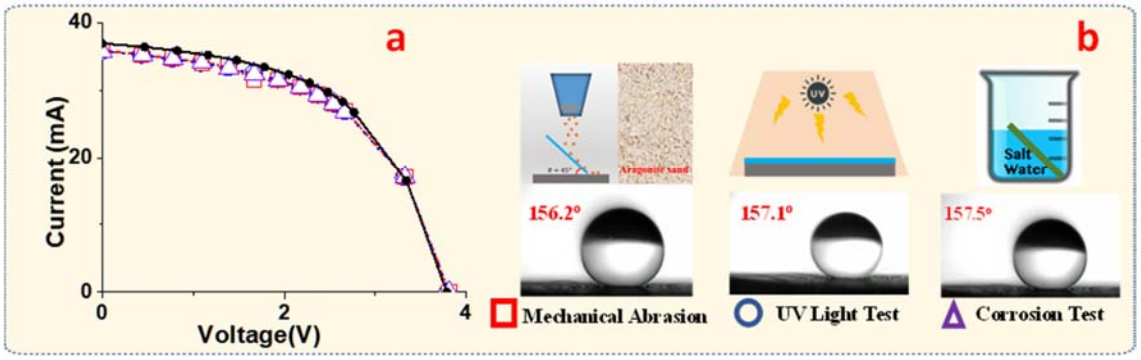

Figure 9 (a) I-V curves and **(b)** contact angles after various controlled durable tests, including mechanical abrasion, a 72-hr UV test under a LED UV lamp, and immersion in different NaCl solutions

ranging from 10 µm to 5 µm impinged the surface released from a height from 10 to 20 cm. Each run lasted five minutes. The surface retained their water-repellency and light trapping effects (I-V curves) after multiple runs from different-sized grains (**Figure 9a and 9b**). Detailed information can find in **Figure S8a** and **S8c**. In comparison, the contact angle over the structured PDMS surface without LSEG decreases to 84.3°, and the solar cell efficiency also decreases significantly (**Figure S8b**). The multilayer graphene film can effectively strengthen and toughen the surface and transfer the stress throughout the structure, making it superior against mechanical wear.[43]

UV degradation test: Most polymer-based nanostructures are prone to be damaged by the UV light. For the long-time usage, i.e., photovoltaics, the nanostructure needs to be continuously exposed to solar irradiation for a long period.[44] If the nanostructure degrades due to UV exposure, it limits its usage for the aforementioned application. Therefore, UV stability is the key. Here, for our ordered-disorder nanostructures, we exposed the surface to UV lamps following the ASTM D4587 standard for 72 hours, equivalent to the one-year daylight UV exposure in Arizona. The surface maintained its water-repellency and light management capability (**Figure 9a and 9b**), showing its resistance to UV. In **Figure S9** we also measured the transmittance of the LSEG-

enabled layer before and after the UV exposure, showing UV resistance. Graphene with high mechanical strength and chemical inertness also has an outstanding anti-irradiation capacity.[45] Hence it is not surprising that the LSEG coating can adequately protect the solar cell from UV exposure.

Corrosion test: The patterned nanostructure can trap air within the surface structures, minimizing the contact with the liquid and leading to non-wetting and anti-corrosion. In order to use air as the corrosion passivation layer, the surface must maintain a Cassie state (trapping air). In other words, the durability in harsh chemical environments such as acid rain or dust dissolved alkaline solution becomes necessary for the successful implementation. In this part, we immersed the surface into two different concentration sodium solution (3% and 5% wt) similar to salt water for three days. **Figure 9a** and **9b** show that the designed LSEG-enabled ordered-disorder nanostructure retained its water repellency and light management. Besides graphene's resistance to corrosion, the PDMS layer is also stable in sodium solutions as shown in **Figure S10**. Therefore, the chemical resistance can be attributed to both the graphene and PDMS.

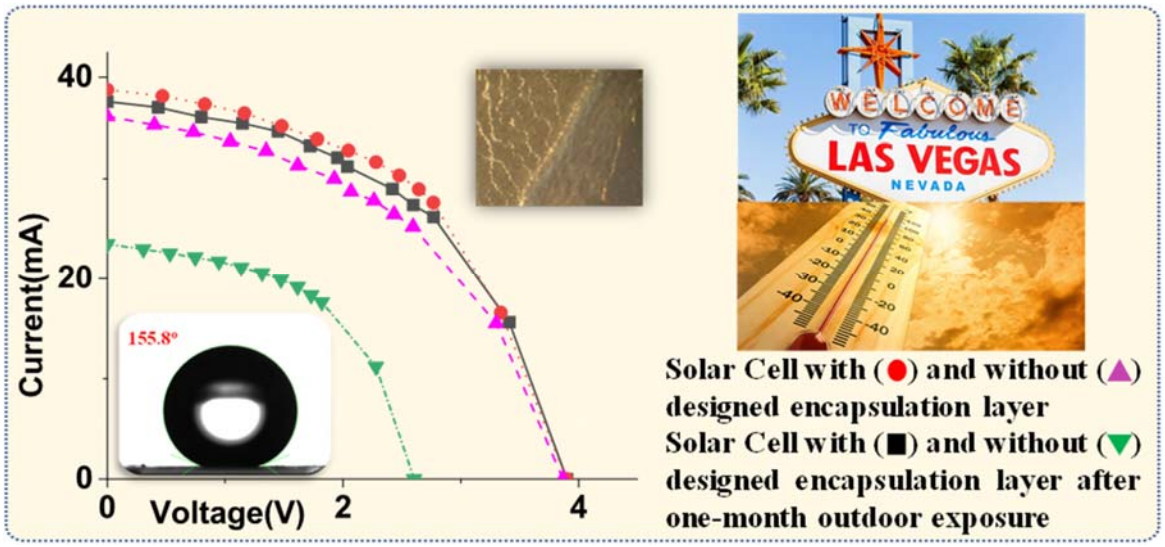

Figure 10 I-V curves and contact angle (lower left) after the one-month outdoor exposure.

Complex real ambient condition impact: Finally, to demonstrate that our designed LSEG-enabled ordered-disorder nanostructure is capable of real-world applications, we conducted outdoor tests. The complex harsh outdoor conditions are a combination of mechanical (dust), chemical (rain), thermal (large daily temperature difference), radiation (UV exposure) durability tests. We left both the solar cell and that coated with our multifunctional nanostructure without caring during the summer of 2017 in Las Vegas. The historical weather data are shown in the supplemental file (**Figure S11 and Table S1**). After the month-long exposure, we measured the current-voltage curve again. Remarkably, the current-voltages curve and the contact angle after outdoor exposure were almost the same as before testing (**Figure 10**), highlighting that our designed coating not only is robust in regarding preserving water repellency but also is extremely durable for light management. For comparison, **Figure 10** shows that the efficiency of the solar cell without the multifunctional coating decreased by 56.2% due to severe degrading when exposed to harsh environments, a common problem for flexible thin film solar cells, significantly limiting its practical applications. The damage caused by environmental degrading is so severe that it can even be witnessed under the microscope (**Figure S12**). In stark contrast, there is no damage observed with our designed LSEG-enabled coating. In other words, besides enhancing the solar cell efficiency, our coating also can serve as the protective layer for thin-film solar cells. Briefly, comprehensive outdoor tests particularly suggest that the thin-film photovoltaic cells, coated with the LSEG-enabled ordered-disorder nanostructure, possess the required mechanical, chemical, thermal, and radiate durability.

3. Conclusion

In summary, the unique fusion of the papillae-like structures (ordered) and multilayer LSEG (disordered), mimicking as many as key characteristics of Viola tricolor petals, not only possessed

the broadband omnidirectional light management with high transmittance and high transmission haze and the prevention of dust accumulation, but also demonstrated exceptional robustness and durability by retaining them under mechanical abrasion, UV exposure, corrosion, and long-time outdoor exposure. Our studies can bridge the critical technological gap and uplift light-management nanostructured materials to the next performance levels by simultaneously improving the durability, longevity, and water repellency.

Finally, we need to point out that our work is bio-inspired. We did not directly replicate or faithfully mimic Viola Tricolor. Instead, by understanding the main physics that makes Viola Tricolor petals possess the exceptional durable light trapping and the prevention of dust accumulation under harsh environments, we employed a hierarchical nanostructure embedded with multilayer LightScribe-etched graphene, capable of omnidirectional light management, which simultaneously demonstrates environmental robustness and resistance to dust accumulation. Because of the bio-inspiring nature of our work, we can go beyond Viola Tricolor and optimize or engineer the performance by changing the design parameters like the underneath pattern and LSEG thickness. Since the underneath pattern can be changed, we can readily replicate other surface patterns including rose petals, random pyramids, inverted pyramid, moth eye and add LSEG layers on top to further improve the efficiency. [46–49]

Experimental Section

Synthesizing the LSEG-enabled nanostructures: PDMS was used to fabricate the transparent nanostructures, mimicking the papillae cell sculptures, with the commercial optic disc as the mold. Here we chose the 5:1 PDMS gel for the following reasons: (1) a higher percentage of the curing agent makes the surface stiffer, and the stiffer PDMS has a higher replication fidelity;[50] (2) it is thermally stable; (3) it swells less due to smaller thermal expansion.

The process was shown in **Figure 3**. In step 1, the PDMS gel was poured onto the Lightscribe optical disc. We need to assure that the PDMS film was perfectly flat and did not cover up the silver ring of the barcode on the LightScribe disc. In addition, the PDMS film should not have stray ends that may interfere with the disc rotation. Then another regular DVD disc as the mold was pressed onto the PDMS gel. In step 2, the PDMS was cured at 70 °C for 45 minutes. Next, the DVD mold is removed, and the DVD structure was replicated on the PDMS (step 3). 100 mg of graphene oxide was dissolved in 27 mL of DI water and ultrasonicated for an hour until the solution was well mixed. In step 4, dipped 15 mL of the dispersion onto the structured PDMS surface and waited for the film to dry at room temperature for 24 hours (step 5). Next, the optical disc was inserted into a standard DVD player and was burned for at least six cycles to effectively reduce the graphene oxide to LSEG (step 6). Finally, the LightScribe disc was removed.

Solar cell attaching process: Thin PDMS gel (~10μm) was spin-coated on the solar cell before attaching the LSEG-enabled PDMS film to eliminate the possible air layer between the PDMS and the solar cell's surface.

Optical characterization: The solar cell and that with the LSEG-enabled ordered-disorder nanostructures were tested in the Newport Sun simulator (940X1 Oriel instrument) with the AM 1.5G sunlight spectrum filter. The current-voltage relations were recorded with the Agilent 34405A and Keithley 6514 system by gradually adjusting the external resistance from 0 to 200 ohms with an interval of 10 ohms. For each resistance, we recorded the current and voltage until they reached a steady state. We measured the I-V curves for different samples of amorphous silicon solar cells in **Figure S13**, showing that there is little variation among them. Also, **Figure S14** shows the I-V curves of three independent measurements of the same solar cell under the same conditions, indicating that the measurement errors are negligible.

Solid particle test: For the mechanical friction test, 20 grams of two types of commercial sands (Caribbean live sand 50μm~150μm and Aragonite sand 0.3mm~1mm) were released to impinge the ordered-disorder nanostructure with a tilted angle 45° from the heights between 10 and 20 cm for three times.

UV test: A 3D UV test chamber was used for the UV tests (shown as **Figure S15**). The test chamber was equipped with four 9 watts UV lamps distributed around the chamber wall. The specification of this test platform was listed in **Table S2**.

Supporting Information

The supporting information is available free of charge on the ACS publication website.

It contains: Photograph of multiple droplets deposited on the surface; The illumination of the flat PDMS and the structured PDMS without the LSEG with lasers; The image of the solar cell with the LSEG-enabled coating; The reflectance of the solar cells with and without the LSEG-enabled coating; The photographs demonstrating that the water droplet slide on the coated layer at a low roll-off angle of 2°; Water droplet wipes the dirt away from the surface with a titled angle of 2°; The contact angles before and after the bending test; The contact angles and the I-V curves before and after the mechanical abrasions; The transmittance before and after the UV test; The transmittance before and after immersion in the NaCl solution; The historical weather data; The images of solar cells before and after the environmental degradation and after mechanical abrasion; The I-V curve of the two different solar cell samples; The I-V curves of three independent measurements; The UV exposure test chamber; The detailed historical weather data; The specifications of the UV test chamber.

AUTHOR INFORMATION

Corresponding Author

*Hui Zhao, hui.zhao@unlv.edu

Author Contributions

S. Zhai and H. Zhao conceived experiments and wrote the paper. S. Zhai and Y. Zhao performed experiments. S. Zhai, Y. Zhao and H. Zhao performed data analysis. All authors have given their approval to the final version of the manuscript.

Funding Sources

This work was, in part, supported by the National Science Foundation under Grant No. ECCS-1509866 and IIA-1301726.

Reference

(1) Scharber, M. C.; Mühlbacher, D.; Koppe, M.; Denk, P.; Waldauf, C.; Heeger, A. J.; Brabec, C. J. Design Rules for Donors in Bulk-Heterojunction Solar Cells—Towards 10 % Energy-Conversion Efficiency. *Adv. Mater.* **2006**, *18*, 789–794.

(2) Zhu, J.; Hsu, C.-M.; Yu, Z.; Fan, S.; Cui, Y. Nanodome Solar Cells with Efficient Light Management and Self-Cleaning. *Nano Lett.* **2010**, *10*, 1979–1984.

(3) Yao, Y.; Yao, J.; Narasimhan, V. K.; Ruan, Z.; Xie, C.; Fan, S.; Cui, Y. Broadband Light Management Using Low-Q Whispering Gallery Modes in Spherical Nanoshells. *Nat. Commun.* **2012**, *3*, 664.

(4) Brongersma, M. L.; Cui, Y.; Fan, S. Light Management for Photovoltaics Using High-Index Nanostructures. *Nat. Mater.* **2014**, *13*, 451–460.

(5) Holman, Z. C.; Filipič, M.; Descoeudres, A.; De Wolf, S.; Smole, F.; Topič, M.; Ballif, C. Infrared Light Management in High-Efficiency Silicon Heterojunction and Rear-Passivated Solar Cells. *J. Appl. Phys.* **2013**, *113*, 013107.

(6) Schmid, M. Review on Light Management by Nanostructures in Chalcopyrite Solar Cells. *Semicond. Sci. Technol.* **2017**, *32*, 043003.

(7) Poortmans, J.; Arkhipov, V.; Wiley InterScience (Online service). *Thin Film Solar Cells : Fabrication, Characterization and Applications*; Wiley, **2006**.

(8) Bernhard, C. G.; Gemne, G.; Moller, A. R. Modification of Specular Reflexion and Light Transmission by Biological Surface Structures. *Q. Rev. Biophys.* **1968**, *1*, 89–105.

(9) Whitney, H. M.; Bennett, K. M. V.; Dorling, M.; Sandbach, L.; Prince, D.; Chittka, L.; Glover, B. J. Why Do so Many Petals Have Conical Epidermal Cells? *Ann. Bot.* **2011**, *108*, 609–616.

(10) Dobzhansky, T.; Hecht, M. K.; Steere, W. C. *Evolutionary Biology : Volume 6*; Springer US, **1995**.

(11) Moyroud, E.; Wenzel, T.; Middleton, R.; Rudall, P. J.; Banks, H.; Reed, A.; Mellers, G.; Killoran, P.; Westwood, M. M.; Steiner, U.; Vignolini S.; Glover, B.J. Disorder in Convergent Floral Nanostructures Enhances Signalling to Bees. *Nature* **2017**, *550*, 469–474.

(12) Zhang, Y.; Sun, T.; Xie, L.; Hayashi, T.; Kawabata, S.; Li, Y. Relationship between the Velvet-like Texture of Flower Petals and Light Reflection from Epidermal Cell Surfaces. *J. Plant Res.* **2015**, *128*, 623–632.

(13) Kay, Q. O. N.; Daoud, H. S.; Stirton, C. H. Pigment Distribution, Light Reflection and Cell Structure in Petals. *Bot. J. Linn. Soc.* **1981**, *83* (1), 57–83.

(14) Kugler, H. Blütenökologische Untersuchungen Mit Hummeln. X. *Planta* **1941**, *32*, 268–285.

(15) Schmager, R.; Fritz, B.; Hünig, R.; Ding, K.; Lemmer, U.; Richards, B. S.; Gomard, G.; Paetzold, U. W. Texture of the Viola Flower for Light Harvesting in Photovoltaics. *ACS Photonics* **2017**, *4*, 2687–2692.

(16) Feng, L.; Zhang, Y.; Xi, J.; Zhu, Y.; Wang, N.; Xia, F.; Jiang, L. Petal Effect: A Superhydrophobic State with High Adhesive Force. *Langmuir* **2008**, *24*, 4114–4119.

(17) Mortazavi, M.; Nosonovsky, M. Polymer Adhesion and Biomimetic Surfaces for Green Tribology. *Green Energy and Technology* **2012**, 173–219.

(18) Schulte, A. J.; Droste, D. M.; Koch, K.; Barthlott, W. Hierarchically Structured Superhydrophobic Flowers with Low Hysteresis of the Wild Pansy (*Viola Tricolor*) – New Design Principles for Biomimetic Materials. *Beilstein J. Nanotechnol.* **2011**, *2*, 228–236.

(19) Ensikat, H. J.; Ditsche-Kuru, P.; Neinhuis, C.; Barthlott, W. Superhydrophobicity in Perfection: The Outstanding Properties of the Lotus Leaf. *Beilstein J. Nanotechnol.* **2011**, *2*, 152–161.

(20) Kunst, L.; Samuels, A. Biosynthesis and Secretion of Plant Cuticular Wax. *Prog. Lipid Res.* **2003**, *42*, 51–80.

(21) Koch, K.; Ensikat, H.-J. The Hydrophobic Coatings of Plant Surfaces: Epicuticular Wax Crystals and Their Morphologies, Crystallinity and Molecular Self-Assembly. *Micron*

2008, *39*, 759–772.

(22) Buschhaus, C.; Jetter, R. Composition and Physiological Function of the Wax Layers Coating Arabidopsis Leaves: β-Amyrin Negatively Affects the Intracuticular Water Barrier. *Plant Physiol.* **2012**, *160*, 1120–1129.

(23) Allen, M. J.; Tung, V. C.; Kaner, R. B. Honeycomb Carbon: A Review of Graphene. *Chem. Rev.* **2010**, *110*, 132–145.

(24) Geim, A. K.; Novoselov, K. S. The Rise of Graphene. *Nat. Mater.* **2007**, *6*, 183–191.

(25) Akinwande, D.; Brennan, C. J.; Bunch, J. S.; Egberts, P.; Felts, J. R.; Gao, H.; Huang, R.; Kim, J.-S.; Li, T.; Li, Y.; Liechti, K.M.; Lu, N.; Park, H.S.; Reed, E.J.; Wang, P.; Yakobson, B.I.; Zhang, T.; Zhang, Y.W.; Zhou, Y.; Zhu, Y. A Review on Mechanics and Mechanical Properties of 2D Materials—Graphene and Beyond. *Extrem. Mech. Lett.* **2017**, *13*, 42–77.

(26) Jiang, H. B.; Zhang, Y. L.; Han, D. D.; Xia, H.; Feng, J.; Chen, Q. D.; Hong, Z. R.; Sun, H. B. Bioinspired Fabrication of Superhydrophobic Graphene Films by Two-Beam Laser Interference. *Adv. Funct. Mater.* **2014**, *24*, 4595–4602.

(27) Shen, J.; Tang, J.; Feng, Y.; Sun, W.; Zhou, B.; Du, A.; Huang, S. Super Black Material from Low-Density Carbon Aerogels with Subwavelength Structures. *ACS Nano* **2016**, *10*, 9123–9128.

(28) Xie, P.; Sun, W.; Liu, Y.; Du, A.; Zhang, Z.; Wu, G.; Fan, R. Carbon Aerogels towards New Candidates for Double Negative Metamaterials of Low Density. *Carbon* **2018**, *129*, 598–606.

(29) Yang, Z.-P.; Hsieh, M.-L.; Bur, J. A.; Ci, L.; Hanssen, L. M.; Wilthan, B.; Ajayan, P. M.;

Lin, S.-Y. Experimental Observation of Extremely Weak Optical Scattering from an Interlocking Carbon Nanotube Array. *Appl. Opt.* **2011**, *50*, 1850.

(30) Xia, Y.; Whitesides, G. M. Soft Lithography. *Annu. Rev. Mater. Sci.* **2002**, *28*, 153–184.

(31) El-Kady, M. F.; Strong, V.; Dubin, S.; Kaner, R. B. Laser Scribing of High-Performance and Flexible Graphene-Based Electrochemical Capacitors. *Science* **2012**, *335*, 1326–1330.

(32) Lin, Y.-C.; Lu, C.-C.; Yeh, C.-H.; Jin, C.; Suenaga, K.; Chiu, P.-W. Graphene Annealing: How Clean Can It Be? *Nano Lett.* **2012**, *12*, 414–419.

(33) Ishikawa, R.; Bando, M.; Morimoto, Y.; Park, S. Y.; Sandhu, A. Patterning of Two-Dimensional Graphene Oxide on Silicon Substrates. *Jpn. J. Appl. Phys.* **2010**, *49*, 06GC02.

(34) Shao, Q.; Tang, J.; Lin, Y.; Zhang, F.; Yuan, J.; Zhang, H.; Shinya, N.; Qin, L.C. Synthesis and Characterization of Graphene Hollow Spheres for Application in Supercapacitors. *J. Mater. Chem. A* **2013**, *1*, 15423.

(35) Hayes, W. I.; Joseph, P.; Mughal, M. Z.; Papakonstantinou, P. Production of Reduced Graphene Oxide via Hydrothermal Reduction in an Aqueous Sulphuric Acid Suspension and Its Electrochemical Behaviour. *J. Solid State Electrochem.* **2015**, *19*, 361–380.

(36) Tung, V. C.; Allen, M. J.; Yang, Y.; Kaner, R. B. High-Throughput Solution Processing of Large-Scale Graphene. *Nat. Nanotechnol.* **2009**, *4*, 25–29.

(37) Munz, M.; Giusca, C. E.; Myers-Ward, R. L.; Gaskill, D. K.; Kazakova, O. Thickness-Dependent Hydrophobicity of Epitaxial Graphene. *ACS Nano* **2015**, *9*, 8401–8411.

(38) Jung, I.; Vaupel, M.; Pelton, M.; Piner, R.; Dikin, D. A.; Stankovich, S.; An, J.; Ruoff, R.

S. Characterization of Thermally Reduced Graphene Oxide by Imaging Ellipsometry. *J. Phys. Chem. C* **2008**, *112*, 8499–8506.

(39) Fang, Z.; Zhu, H.; Yuan, Y.; Ha, D.; Zhu, S.; Preston, C.; Chen, Q.; Li, Y.; Han, X.; Lee, S.; et al. Novel Nanostructured Paper with Ultrahigh Transparency and Ultrahigh Haze for Solar Cells. *Nano Lett.* **2014**, *14*, 765–773.

(40) Stradi, D.; Barja, S.; Díaz, C.; Garnica, M.; Borca, B.; Hinarejos, J. J.; Sánchez-Portal, D.; Alcamí, M.; Arnau, A.; Vázquez de Parga, A. L.; Miranda, R.; Martin, F. Lattice-Matched versus Lattice-Mismatched Models to Describe Epitaxial Monolayer Graphene on Ru(0001). *Phys. Rev. B* **2013**, *88*, 245401.

(41) Stolyarova, E.; Stolyarov, D.; Bolotin, K.; Ryu, S.; Liu, L.; Rim, K. T.; Klima, M.; Hybertsen, M.; Pogorelsky, I.; Pavlishin, I.; Kusche, K.; Hone, J.; Kim, P.; Stormer, H. L.; Yakimenko, V.; Flynn, G. Observation of Graphene Bubbles and Effective Mass Transport under Graphene Films. *Nano Lett.* **2009**, *9*, 332–337.

(42) Krasnov, H.; Katra, I.; Koutrakis, P.; Friger, M. D. Contribution of Dust Storms to PM $_{10}$ Levels in an Urban Arid Environment. *J. Air Waste Manage. Assoc.* **2014**, *64*, 89–94.

(43) Nine, M. J.; Cole, M. A.; Tran, D. N. H.; Losic, D. Graphene: A Multipurpose Material for Protective Coatings. *J. Mater. Chem. A* **2015**, *3*, 12580–12602.

(44) Jordan, D. C.; Kurtz, S. R. Photovoltaic Degradation Rates-an Analytical Review. *Prog. Photovoltaics Res. Appl.* **2013**, *21*, 12–29.

(45) Fan, X.; Wang, L. Graphene with Outstanding Anti-Irradiation Capacity as Multialkylated Cyclopentanes Additive toward Space Application. *Sci. Rep.* **2015**, *5*, 12734.

(46) Jošt, M.; Köhnen, E.; Morales-Vilches, A. B.; Lipovšek, B.; Jäger, K.; Macco, B.; Al-Ashouri, A.; Krč, J.; Korte, L.; Rech, B.; Schlatmann, R.; Topic, M.; Stannowski, B.; Albrecht, S. Textured Interfaces in Monolithic Perovskite/Silicon Tandem Solar Cells: Advanced Light Management for Improved Efficiency and Energy Yield. *Energy Environ. Sci.* **2018**, *11*, 3511–3523.

(47) Kang, S. M.; Jang, S.; Lee, J.-K.; Yoon, J.; Yoo, D.-E.; Lee, J.-W.; Choi, M.; Park, N.-G. Moth-Eye TiO_2 Layer for Improving Light Harvesting Efficiency in Perovskite Solar Cells. *Small* **2016**, *12*, 2443–2449.

(48) Choo, S.; Choi, H.-J.; Lee, H. Replication of Rose-Petal Surface Structure Using UV-Nanoimprint Lithography. *Mater. Lett.* **2014**, *121*, 170–173.

(49) Dudem, B.; Heo, J. H.; Leem, J. W.; Yu, J. S.; Im, S. H. $CH_3NH_3PbI_3$ Planar Perovskite Solar Cells with Antireflection and Self-Cleaning Function Layers. *J. Mater. Chem. A* **2016**, *4*, 7573–7579.

(50) Zhai, S.; Zhao, H. Enhancement of Sensitivity of the Solution-Phase Localized Surface Plasmon by a Nanostructured Substrate. *MRS Adv.* **2016**, *1*, 2059–2064.

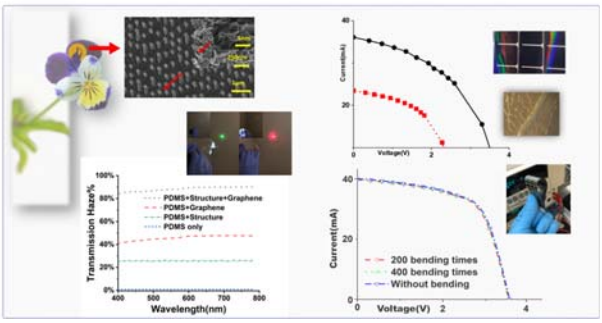

Cover Art (TOC)